Deficiency of liver Comparative Gene Identification-58 causes steatohepatitis and fibrosis in mice

Feng Guo,* Yinyan Ma,*,† Anil K. G. Kadegowda,† Jenna L. Betters,††† Ping Xie,* George Liu,§ Xiuli Liu,** Hongming Miao,† Juanjuan Ou,† Xiong Su,†† Zhenlin Zheng,§§ Bingzhong Xue,*** Hang Shi,*** and Liqing Yu[1],*,†

Departments of Biochemistry* and Plastic Surgery,§§ Wake Forest University School of Medicine, Winston-Salem, NC; Department of Animal and Avian Sciences,† University of Maryland, College Park, MD; Institute of Cardiovascular Sciences and Key Laboratory of Molecular Cardiovascular Sciences,§ Ministry of Education, Peking University Health Science Center, Beijing, China; Department of Anatomic Pathology,** Cleveland Clinic, Cleveland, OH; Nutritional Sciences and Departments of Medicine, Cell Biology, and Physiology,†† Washington University School of Medicine, St. Louis, MO; Department of Biology,*** Georgia State University, Atlanta, GA; and Department of Pathology,††† Section on Lipid Sciences, Wake Forest University School of Medicine, Winston-Salem, NC

Abstract Triglyceride (TG) accumulation in hepatocytes (hepatic steatosis) preludes the development of advanced nonalcoholic fatty liver diseases (NAFLDs) such as steatohepatitis, fibrosis, and cirrhosis. Mutations in human Comparative Gene Identification-58 (CGI-58) cause cytosolic TG-rich lipid droplets to accumulate in almost all cell types including hepatocytes. However, it is unclear if CGI-58 mutation causes hepatic steatosis locally or via altering lipid metabolism in other tissues. To directly address this question, we created liver-specific CGI-58 knockout (LivKO) mice. LivKO mice on standard chow diet displayed microvesicular and macrovesicular panlobular steatosis, and progressed to advanced NAFLD stages over time, including lobular inflammation and centrilobular fibrosis. Compared with CGI-58 floxed control littermates, LivKO mice showed 8-fold and 52-fold increases in hepatic TG content, which was associated with 40% and 58% decreases in hepatic TG hydrolase activity at 16 and 42 weeks, respectively. Hepatic cholesterol also increased significantly in LivKO mice. At 42 weeks, LivKO mice showed increased hepatic oxidative stress, plasma aminotransferases, and hepatic mRNAs for genes involved in fibrosis and inflammation, such as α-smooth muscle actin, collagen type 1 α1, tumor necrosis factor α, and interleukin-1β. In conclusion, CGI-58 deficiency in the liver directly causes not only hepatic steatosis but also steatohepatitis and fibrosis.—Guo, F., Y. Ma, A. K. G. Kadegowda, J. L. Betters, P. Xie, G. Liu, X. Liu, H. Miao, J. Ou, X. Su, Z. Zheng, B. Xue, H. Shi, and L. Yu. **Deficiency of liver Comparative Gene Identification-58 causes steatohepatitis and fibrosis in mice.** *J. Lipid Res.* 2013. **54:** 2109–2120.

Supplementary key words triglyceride hydrolysis • lipase • fatty liver • CGI-58

Mammals store excess triglyceride (TG) in the large lipid droplet (LD) of white adipose tissue. During a period of starvation or increased energy demand, the stored TG is used as an energy source via a process called lipolysis. Excessive lipid accumulation in nonadipose tissues ("ectopic" fat deposition) is lipotoxic (1). Increased TG accumulation in liver hepatocytes is a hallmark of nonalcoholic fatty liver disease (NAFLD) (2, 3). NAFLD is the most common liver disease in the United States (4–6). In the general population, the estimated prevalence of NAFLD is as high as 24% (6). The highest estimates of NAFLD are among obese individuals after bariatric surgery, which range from 84% to 96% of all patients undergoing this procedure (6). It is estimated that 17–33% of Americans may have hepatic steatosis (5), a condition that is often associated with insulin resistance, type 2 diabetes, and central obesity. The prevalence of NAFLD is increasing worldwide and is expected to more than double by the year 2025 (5).

NAFLD includes a spectrum of liver pathological changes ranging from simple hepatic steatosis to advanced abnor-

malities such as nonalcoholic steatohepatitis (NASH), fibrosis, and cirrhosis (7, 8). In some individuals, hepatic steatosis never progresses to NASH (9, 10). A two-hit hypothesis has been proposed in the pathogenesis of NASH (10), whereby steatosis is the first "hit". Steatosis can be induced by dietary excess, insulin resistance, endoplasmic reticulum (ER) stress, and other factors. The second hit may include multiple factors such as fat-induced oxidative stress, mitochondrial dysfunction, elevated production of reactive oxygen species, and proinflammatory cytokines. This second hit is believed to ultimately result in hepatocellular damage, inflammation, and fibrosis.

Due to ethical constraints in procuring human tissues, animal models are required for exploring mechanisms and prevention of NAFLD progression. Many animal models for NAFLD have been created (11–13), but limited research has been focused on the role of hepatocyte TG hydrolysis in the development of NAFLD. Recently, adipose triglyceride lipase (ATGL) was shown to play an important role in liver TG hydrolysis (14–16). Global or liver-specific inactivation of ATGL in mice results in hepatic steatosis (17, 18), whereas hepatic overexpression of ATGL in *ob/ob* mice decreases liver steatosis (19, 20), suggesting an important role of intracellular TG hydrolysis in preventing fat deposition in the liver.

Comparative gene identification-58 (CGI-58) (21), also known as α/β-hydrolase domain-containing protein 5, is a member of α/β-hydrolase fold protein family (22, 23). The protein is ubiquitously expressed (24–26). In humans, the CGI-58 gene contains seven exons encoding a 349aa protein of $\sim$39 kDa (27). CGI-58 protein lacks a serine residue in the canonical lipase catalytic domain (GXSXG) (23), and possesses no lipid hydrolase activity (23, 25, 28). An elegant study by Dr. Rudolf Zechner and associates has demonstrated that CGI-58 robustly stimulates the in vitro TG hydrolase activity of ATGL (25). This study defined CGI-58 as a coactivator of a lipase, and established a direct role of CGI-58 in promoting intracellular TG hydrolysis.

Mutations in human CGI-58 cause Chanarin-Dorfman syndrome (CDS) (27, 29, 30), an autosomal recessive neutral lipid storage disease associated with ichthyosis (thickened dry skin) and accumulation of TG-rich cytoplasmic LDs in most cell types, including leukocytes (Jordan's anomaly) (31), hepatocytes, myocytes, cells in the epidermis and dermis, and intestinal mucosa (29, 30, 32, 33). Patients with CDS often have hepatomegaly, myopathy, microcephaly, cataracts, hearing loss, ataxia, mild mental retardation, and short stature (29, 30, 32–40).

Interestingly, mutations in human and mouse ATGL also cause a neutral lipid storage disease (17, 41). However, phenotypic differences exist between CGI-58 and ATGL mutations. ATGL mutations in humans cause no ichthyosis (41), whereas CGI-58 mutations in humans always cause ichthyosis (27, 41). While whole-body ATGL knockout mice are viable, global CGI-58 knockout mice die within 16 h after birth due to a defect in skin barrier function (42). These observations suggest that CGI-58 has functions beyond ATGL activation.

Our previous studies have shown that antisense oligonucleotide (ASO)-mediated knockdown of CGI-58 in multiple tissues (liver, fat, and macrophages) of adult mice induces hepatic steatosis (43), but we did not know if this was a result of local effect of CGI-58 knockdown, or liver response to the effects of CGI-58 knockdown in other tissues such as fat and macrophages. To identify the role of CGI-58 in hepatic lipid metabolism and in the development of NAFLD, we generated liver-specific CGI-58 knockout (LivKO) mice. We found that liver-specific deletion of CGI-58 reduces hepatic TG hydrolase activity and directly causes progressive NAFLD. Our findings establish liver CGI-58 as a crucial hydrolytic factor against the progression of NAFLD, and suggest that inhibition of liver TG hydrolysis may be a major risk factor for NAFLD.

MATERIALS AND METHODS

Creation of CGI-58 floxed mice and LivKO mice

The gene targeting construct was assembled from two DNA segments of the mouse *CGI-58* gene that were amplified by PCR from the genomic DNA of R1 mouse embryonic stem (ES) cells (44) (kindly provided by Dr. Andras Nagy at Samuel Lunenfeld Research Institute, Mount Sinai Hospital, and University of Toronto, Toronto, Ontario, Canada). The 5′ homologous arm (1.04 kb) including part of the second intron was amplified and subcloned into *Xho*I site of the pJB1 gene-targeting vector (45). The 3′ homologous arm (8.3 kb) including part of intron 2, entire exon 3, and most of intron 3 was amplified and subcloned into pGEM-T Easy Vector (Promega). The third *LoxP* site was inserted into an *EcoR*V site in the intron 3 sequence of the cloned 3′ homologous arm. The 3′ homologous arm and the correct orientation of the third *LoxP* site were confirmed by DNA sequencing. The entire 3′ homologous arm was then released from pGEM-T Easy Vector and subcloned into *Not*I site of the pJB1 vector into which the 1.04 kb 5′ homology arm was already inserted.

The gene-targeting construct was linearized, purified, and then introduced into R1 mouse ES cells. After positive and negative selections, ES cell clones were screened for homologous recombination by PCR and Southern blotting. Five correctly targeted clones were identified, and three of them were injected into C57BL/6 blastocysts at the Transgenic Mouse Core Facility of Wake Forest University Health Sciences. Chimeric male mice were mated with C57BL/6 female mice and the germ-line transmission was assessed by PCR genotyping. Mice with the targeted allele were mated with 129S4/Sv-Tg-Gt(ROSA)26Sortm1(FLP1) dym mice (Jackson Laboratory, stock #003946) to delete the *FRT* site-flanked neomycin cassette using the transgene-derived Flp recombinase. The progeny was then crossed with C57BL/6 mice to segregate the *Flp* transgene, thereby creating heterozygous CGI-58 floxed (CGI-58$^{f/+}$) mice harboring an allele in which exon 3 (the largest exon in the mouse *CGI-58* gene) is flanked by two *LoxP* sites (**Fig. 1A**).

CGI-58$^{f/+}$ mice were then crossed with Alb-cre mice of C57BL/6J background [B6.Cg-Tg(Alb-cre)21Mgn/J, stock #003574, The Jackson Laboratory] to generate CGI-58$^{f/+}$/Alb-cre mice and CGI-58$^{f/+}$ mice, which had 93.75% C57BL/6 background. Further crossing of these two genotypes generated homozygous CGI-58$^{f/+}$ mice with Alb-cre transgene (LivKO) mice and homozygous CGI-58$^{f/+}$ mice without Alb-cre transgene (control) mice.
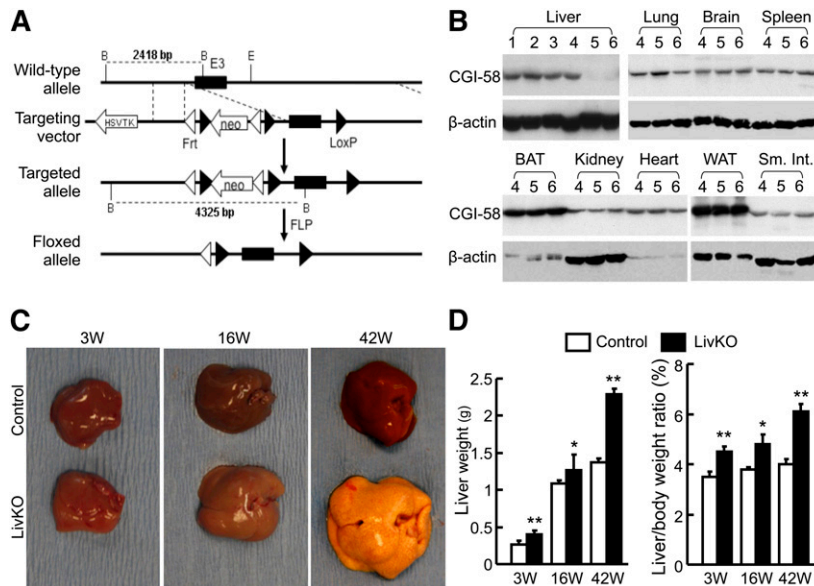
Fig. 1. Liver-specific deletion of CGI-58 causes hepatomegaly in mice. A: A diagram showing strategy used to generate CGI-58[f/+] mice. B: Western blots showing liver-specific ablation of CGI-58 protein in LivKO mice. 1, wild-type mouse; 2, wild-type mouse with albumin-Cre transgene; 3, homozygous CGI-58[f/+] mouse; 4, wild-type mouse with albumin-Cre transgene; 5,6, LivKO mice. C: Gross appearance of livers in LivKO and control mice of different ages. D: Liver weight and liver-to-body weight ratios of LivKO and control male mice (n = 4–5). 3W, 3 weeks; 16W, 16 weeks; 42W, 42 weeks. *$P < 0.05$; **$P < 0.01$.

Male CGI-58 LivKO mice and control littermates were fed a normal chow diet (Prolab RMH 3000, LabDiet; Brentwood, MO). All animal procedures were approved by the Institutional Animal Care and Use Committee at Wake Forest University Health Sciences and at University of Maryland in compliance with animal welfare assurance.

Western blotting

A total of 50 µg of tissue homogenate was subjected to 10% SDS-PAGE and the proteins were then transferred to nitrocellulose membranes. The membranes were blocked with 5% nonfat milk in phosphate-buffered saline containing 0.05% Tween 20, and probed with primary antibodies, followed by secondary antibodies. After incubation with ECL (Pierce), the membranes were exposed to X-ray films or read under a Bio-Rad imaging system.

The mouse monoclonal antibody to human CGI-58 was from Abnova (catalog #H00051099-M01; Clone 1F3). This antibody cross-reacts with mouse CGI-58 (43). ATGL antibody was purchased from Cayman Chemical Company (catalog #10006409). Except anti-phospho-IRE1α(pSer724) antibody, which was from Thermo Scientific (catalog #PA1-16927), all other antibodies against ER stress markers (ER Stress Antibody Sampler Kit #9956) as well as those against total Akt (C67E7) (catalog #4691), phospho-Akt(Thr308) (C31E5E) (catalog #2965), α-tubulin (catalog #3873), and β-actin (catalog #3700) were from Cell Signaling Technology.

RNA extraction and quantitative real-time PCR

Total RNA was extracted from tissues by homogenizing snap-frozen tissue samples in TRIzol reagent (Invitrogen). The cDNA was synthesized from 2 µg of total RNA using the SuperScript First Strand system (Invitrogen) and random hexamer primers. The resultant cDNA was used as a template for quantitative real-time PCR (qPCR) as described previously (46). Cyclophilin or glyceraldehyde-3-phosphate dehydrogenase (GAPDH) was used as an internal control. All qPCR primer sequences are available upon request.

VLDL-TG production assay

The mice on regular chow diet were fasted for 4 h, followed by tail vein injection of 500 mg/kg body weight (BW) Triton WR1339 (Tyloxapol, Sigma-Aldrich, catalog #T0307) to inhibit plasma TG hydrolysis mediated by lipoprotein lipase. Blood (∼20 µl) was collected before Triton injection (at 0 min) as well as at 30, 60, 90, and 120 min after Triton injection. Plasma TG concentrations were determined enzymatically and plotted as a function of time.

Determination of plasma and hepatic lipids

Plasma samples were collected by submandibular vein puncture. Plasma β-hydroxybutyrate (Stanbio Laboratory, Boerne, TX) and nonesterified fatty acids (NEFAs) (HR Series NEFA-HR, Wako Diagnostics, Richmond, VA) were measured following the manufacturer's instructions. Plasma concentrations of total cholesterol (TC), phospholipids (PLs), and TG were analyzed using the TC, PL (Wako), and TG (Sigma) enzymatic assay kits, respectively. Plasma alanine transaminase (ALT) and aspartate transaminase (AST) activities were measured using commercial kits (Point Scientific, Inc., Canton, MI).

After a 4 h fast during the daylight cycle, mice were euthanized and tissues were removed and snap-frozen in liquid nitrogen for lipid analysis as we have described previously (47, 48).

Measurements of hepatic TG hydrolase, FA oxidation, and cholesterol ester hydrolase activities

Liver TG hydrolase activity and FA oxidation were measured exactly as we have described previously (43, 49). Hepatic cholesterol ester (CE) hydrolase activity was measured as described by Holm and Osterlund (50). Briefly, cholesterol esterase activity was assayed using cholesterol [1-^{14}C]oleate (American Radiolabeled Chemicals) as a substrate. The substrate emulsion particles (3 ml) consisted of 0.88 mg of cholesterol oleate, 20 µCi of cholesterol [1-^{14}C]oleate, and 1.065 mg of PLs. The lipid mixture, initially dried under N_2 to remove the residual solvents, was

added to 1.5 ml of 0.1 M potassium phosphate buffer, pH 7.0, warmed to 37°C, and sonicated on ice (2 cycles, 1 min, with 1 min interval). Additional 0.75 ml of 0.1 M potassium phosphate buffer, pH 7.0, was added and sonicated (4 cycles, 30 s, with 30 s interval) on ice. At this point, 0.75 ml of 20% BSA in 0.1 M potassium phosphate buffer, pH 7.0, was added to the substrate emulsion and mixed well. For each assay, 100 μl of substrate emulsion particles were mixed with 100 μl of sample (consisting of 100 μg liver homogenate protein in 20 mM potassium phosphate, 1 mM EDTA, 1 mM dithioerythritol, 0.02% BSA, pH 7.0) and incubated for 60 min at 37°C in a water bath. The reaction was terminated by addition of 3.25 ml of extraction mixture (methanol:chloroform:heptane, 10:9:7) and 1.05 ml of 0.1 M potassium carbonate, 0.1 M boric acid, pH 10.5. The mixture was vortexed for 10 s and centrifuged at 800 g for 20 min for phase separation. The upper phase (1 ml) containing released [1-^{14}C]oleate was counted in 10 ml of Ready-Safe liquid scintillation cocktail in a liquid scintillation counter.

Liver histopathology

Liver specimens were fixed in 10% buffered formalin and processed for hematoxylin and eosin (H and E) and trichrome staining by the Clinical Pathology Lab in the Department of Pathology at Wake Forest University School of Medicine.

Glucose and insulin tolerance tests

For the glucose tolerance test (GTT), mice were fasted overnight. Each mouse was then weighed. After measuring the baseline blood glucose level via a tail nick using a OneTouch Ultra glucometer (Lifescan Canada Ltd.), a 20% glucose solution was injected intraperitoneally at 1.5 mg/g BW. Blood glucose levels were measured at 15, 30, 60, and 120 min after glucose injection. For the insulin tolerance test (ITT), mice were fasted 6 h during the daylight cycle. After the measurement of the baseline blood glucose level, the mice were injected intraperitoneally with recombinant human insulin at 0.75 mU/g BW, and their blood glucose concentrations were determined at 15, 30, 60, and 120 min post insulin administration.

Hepatic oxidative stress

Hepatic superoxide (O_2^-) levels were determined on 10 μm of liver cryosections with the oxidative fluorescent dye dihydroethidium (DHE) (Molecular Probes), and then imaged under a fluorescence Leica microscope equipped with a deconvolution system. Hepatic levels of the lipid peroxidation product malondialdehyde (MDA) were measured as thiobarbituric acid reactive substrates (TBARS) using the TBARS Assay Kit (Cayman Chemical Co.). Hepatic redox environment was determined by measuring the glutathione (GSH)/oxidized glutathione (GSSG) ratio using the Glutathione Assay Kit (Cayman Chemical Co.).

ER stress

Hepatic ER stress was assessed by Western blotting and qPCR of ER stress markers as well as by measuring XBP-1 splicing as described by Deng et al. (51)

Statistical analysis

Values are expressed as means ± SEM. Statistical differences were analyzed using two-tailed Student's t-test. $P < 0.05$ was considered as significant.

RESULTS

Liver-specific deletion of CGI-58 protein in LivKO Mice

Albumin-cre transgenic mice have been widely used to knock out gene expression specifically in the liver of floxed mice (52). To confirm liver-specific disruption of CGI-58 in our model, CGI-58 Western blotting was performed with liver homogenates from the following mice: wild-type mice, wild-type mice expressing albumin-cre transgene in one allele, homozygous CGI-58$^{f/+}$ mice, and homozygous CGI-58$^{f/+}$ mice expressing albumin-cre transgene in one allele (LivKO). As expected, CGI-58 protein expression was specifically disrupted in the liver of CGI-58 LivKO mice. Albumin-cre transgene did not affect CGI-58 expression in all other tissues examined, including heart, brain, lung, kidney, epididymal fat, and brown fat (Fig. 1B). Because CGI-58 protein levels were indistinguishable in the three control groups, we crossed the homozygous CGI-58$^{f/+}$ (control) mice to LivKO mice, and generated LivKO mice and their control littermates for all of the following experiments.

LivKO mice display hepatomegaly

CGI-58 LivKO mice appeared normal grossly and showed no defects in skin and body shape. They gained similar weight as their littermate controls (data not shown). The mice were sacrificed at different ages (3 weeks, 16 weeks, and 42 weeks) for gross and histological examinations. Except for the liver, there was no difference in gross inspection of major organs. LivKO livers appeared pale and yellowish. Hepatomegaly was evident in LivKO mice, which became more obvious over time (Fig. 1C). The 42-week-old LivKO livers were dramatically enlarged and hardened, and showed rare small white nodules on the yellowish surface (signs of fatty liver and fibrosis). The liver weight and liver-to-body weight ratio increased significantly in all LivKO mice, regardless of age (Fig. 1D).

LivKO mice develop significant hepatic steatosis

To examine histopathological alterations of LivKO livers, liver sections were stained by H and E. The 3-week-old LivKO mice started to show scattered hepatocytes with unilocular vacuoles, indicative of cytosolic LD formation (**Fig. 2A**). Both small and large vacuoles were evident in 16-week-old and 42-week-old mice. There were more foamy hepatocytes in 42-week-old versus 16-week-old LivKO mice, and this foamy appearance resulted from accumulation of many small vacuoles in a hepatocyte.

These findings from H and E staining suggested that LivKO livers developed both microvesicular and macrovesicular steatosis. The macrovesicular steatosis was primarily located in the zone 1 and panlobular region, whereas the microvesicular steatosis was predominant around zones 3 and 2.

Consistently with liver steatosis, hepatic TG content increased dramatically in LivKO mice relative to controls (Fig. 2B). At 16 weeks, LivKO mice accumulated over 8-fold more TG in the liver (1,112 ± 179 μg/mg protein in LivKO vs. 135 ± 18 μg/mg protein in control). At 42 weeks of age, hepatic TG increased ∼52-fold in LivKO mice (4,123 ± 283 μg/mg protein in LivKO vs. 79 ± 15 μg/mg protein in control), indicating progressive hepatic TG deposition with aging.

Hepatic FA composition analysis showed that most FA species of TG increased 2- to 14-fold in 12-week-old LivKO
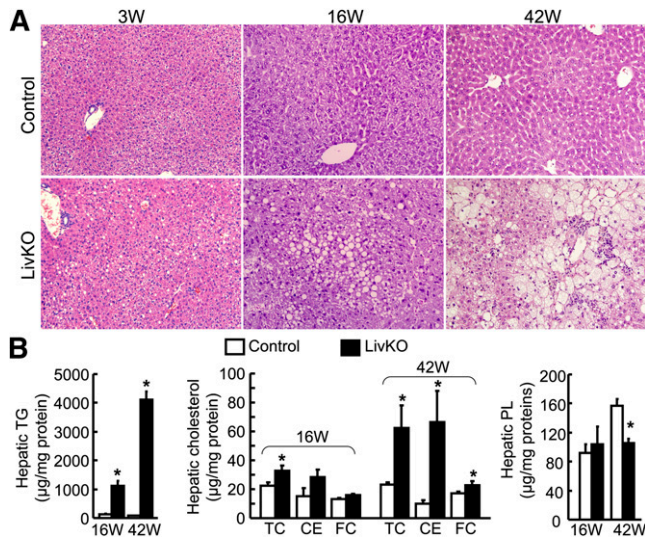
Fig. 2. LivKO mice develop progressive hepatic steatosis. A: H and E staining of liver sections from LivKO and control male mice (200× magnification). B: Hepatic lipid contents in LivKO and control male mice (n = 4–5). CE mass was calculated by multiplying the mass difference between TC and FC by 1.67. 3W, 3 weeks; 16W, 16 weeks; 42W, 42 weeks. *$P < 0.05$.

male mice (**Table 1**). The total hepatic diacylglycerol (DAG) content was almost the same between the two genotypes, while a few FA species of DAG decreased in LivKO mice, such as C14:0, C15:0, and C18:3 (**Table 2**). The hepatic total TG/DAG ratio increased from 48 in control mice to 499 in LivKo mice. These data indicate that liver CGI-58 deficiency in mice on chow diet specifically causes hepatic accumulation of TG, but not DAG.

Intriguingly, the hepatic content of TC also increased significantly in 16-week-old LivKO mice (32.9 ± 3.5 µg/mg protein for LivKO vs. 22.4 ± 2.6 µg/mg protein for control) (Fig. 2B) and this increase was exacerbated in 42-week-old LivKO mice (62.5 ± 15.6 µg/mg protein for LivKO vs. 23.1 ± 1.8 µg/mg protein for control). Significant increases in hepatic free cholesterol (FC) and CE mass [CE mass =

(TC – FC) × 1.67] were observed in LivKO mice at 42 weeks. The hepatic PL content was similar between LivKO and control mice at 16 weeks, but significantly reduced in LivKO mice at 42 weeks (157 ± 10 µg/mg protein in LivKO vs. 105 ± 6 µg/mg protein in control) (Fig. 2B).

LivKO mice produce VLDL-TG normally and have normal plasma lipids

We have previously shown that ASO-mediated simultaneous knockdown of CGI-58 in liver, fat, and macrophages of adult mice inhibits hepatic VLDL-TG secretion (53). To determine if liver-specific inactivation of CGI-58 has the same effect, we measured hepatic VLDL-TG production by the Triton block technique in 8–10 week old male mice on chow diet. Interestingly, we found no changes in hepatic VLDL-TG production in LivKO mice (**Fig. 3A**). To examine whether CGI-58 deficiency-induced liver abnormalities influence systemic lipid homeostasis, we measured plasma concentrations of TG, TC, CE, FC, and PLs. Compared with control mice, no significant changes were observed for these lipids in the plasma of both 16-week-old and 42-week-old LivKO mice (Fig. 3B).

The plasma concentration of NEFA is an indicator of fat lipolysis and utilization during fasting. Hepatic-specific inactivation of CGI-58 did not alter plasma concentrations of NEFA during both fed and fasted states (Fig. 3C). When mRNA levels in epididymal fat pads were examined for genes involved in adipose lipolysis, lipogenesis, and adipogenesis, we did not observe a consistent direction in changes of these genes in LivKO mice. Specifically no significant changes were seen for lipoprotein lipase (LPL), ATGL, hormone sensitive lipase, peroxisome proliferator-activated receptor (PPAR)-γ, sterol regulatory element binding protein (SREBP)-1c, fatty acid synthase (FAS), mitochondrial glycerol-3-phosphate-acyltransferase (GPAT), and diacylglycerol acyltransferase (DGAT) 1, though a lipolytic inhibitor G_0G_1 switch gene 2 (GOS2) (54) and a lipogenic gene stearoyl-CoA desaturase-1 (SCD-1) were significantly downregulated (Fig. 3D). Additionally, we did not see a change

TABLE 1. Hepatic contents of total TG and FA species of TG in 12-week-old LivKO and control male mice on chow diet

TG-FA Species (µmol/g wet tissue)	Control	LivKO	P	Folder Change LivKO versus Control
C14:1	0.27 ± 0.11	0.11 ± 0.02	0.17	0.40
C14:0	0.67 ± 0.19	3.19 ± 0.46	<0.01	4.74
C15:0	0.45 ± 0.15	0.56 ± 0.12	0.57	1.26
C16:1	1.15 ± 0.07	14.16 ± 1.86	<0.01	12.33
C16:0	13.19 ± 1.19	131.40 ± 5.93	<0.01	9.96
C17:0	0.14 ± 0.01	0.77 ± 0.08	<0.01	5.45
C18:3	0.37 ± 0.10	0.99 ± 0.16	<0.01	2.67
C18:2	7.23 ± 1.19	102.38 ± 5.04	<0.01	14.17
C18:1n9	13.62 ± 1.30	165.89 ± 8.62	<0.01	12.18
C18:1	1.08 ± 0.25	12.80 ± 1.18	<0.01	11.87
C18:0	1.45 ± 0.31	7.41 ± 0.76	<0.01	5.12
C20:4n6	0.67 ± 0.11	4.62 ± 0.72	<0.01	6.94
C20:3n6	0.54 ± 0.22	1.70 ± 0.40	<0.01	3.14
C20:2	0.25 ± 0.06	1.36 ± 0.27	<0.01	5.55
C20:1 + C20:3n3	0.27 ± 0.07	1.23 ± 0.27	<0.01	4.62
C20:0	0.29 ± 0.08	0.15 ± 0.02	0.11	0.52
SUM-FFA	41.63 ± 4.04	448.72 ± 21.36	<0.01	10.78
Total TG (µmol/g wet tissue)	13.88 ± 1.35	149.57 ± 7.12	<0.01	10.78

Values are expressed as mean ± SEM; n = 5.

TABLE 2. Hepatic contents of total DAG and FA species of DAG in 12-week-old LivKO and control male mice on chow diet

DAG-FA Species (nmol/g wet tissue)	Control	LivKO	P	Folder Change LivKO versus Control
C14:0	5.93 ± 0.84	1.14 ± 0.17	<0.01	0.19
C15:0	9.38 ± 1.14	0.95 ± 0.18	<0.01	0.10
C16:1	12.04 ± 1.42	11.09 ± 1.76	0.69	0.92
C16:0	210.21 ± 14.09	273.14 ± 29.45	0.09	1.30
C17:0	5.94 ± 0.58	4.45 ± 0.52	0.09	0.75
C18:3	1.10 ± 0.23	0.09 ± 0.01	<0.01	0.08
C18:2	100.14 ± 8.06	81.03 ± 6.24	0.10	0.81
C18:1n9	141.18 ± 9.93	130.45 ± 15.82	0.58	0.92
C18:1	14.38 ± 0.52	12.39 ± 1.03	0.12	0.86
C18:0	48.65 ± 4.29	55.42 ± 4.80	0.32	1.14
C20:4n6	11.04 ± 2.04	13.94 ± 1.02	0.24	1.26
C20:3n6	2.35 ± 0.48	3.02 ± 0.27	0.26	1.29
C20:2	3.15 ± 0.51	3.45 ± 0.99	0.80	1.10
C20:1 + C20:3n3	5.76 ± 1.48	6.81 ± 0.92	0.57	1.18
C20:0	1.86 ± 0.64	1.75 ± 0.25	0.87	0.94
SUM-FFA	573.10 ± 21.79	599.13 ± 54.22	0.67	1.05
Total DAG (nmol/g wet tissue)	286.55 ± 10.89	299.56 ± 27.11	0.67	1.05

Values are expressed as mean ± SEM; n = 5.

in the epididymal fat pad-to-body weight ratio between the two genotypes. Nonetheless, detailed metabolic studies may be needed in the future to definitively define whether the downregulation of GOS2 and SCD-1 represents increased adipose lipolysis and reduced lipogenesis in response to hepatic CGI-58 deficiency.

LivKO liver has reduced TG hydrolase activity and FA oxidation

To examine whether the increased hepatic deposition of TG and cholesterol in LivKO mice was a result of increased biosynthesis of these lipids, we measured hepatic mRNA

levels of genes related to lipogenesis, cholesterologenesis, and regulation of FA oxidation, including SREBP-1c, acetyl-CoA carboxylase 1, DGAT2, GPAT, SREBP-2, 3-hydroxy-3-methylglutaryl (HMG)-CoA reductase, PPAR-α, PPAR-γ coactivator 1α, and fibroblast growth factor 21. We found no significant changes in hepatic expression levels of mRNAs for these genes (**Fig. 4A**). In contrast, hepatic TG hydrolase activity decreased $\sim$40% in 16-week-old LivKO mice (24.2 ± 0.46 nmol FFA/h/mg protein) relative to control mice (40.5 ± 2.04 nmol FFA/h/mg protein) (Fig. 4B). In 42-week-old groups, hepatic TG hydrolase activity in LivKO mice dramatically decreased $\sim$58% (18.6 ± 0.73 nmol
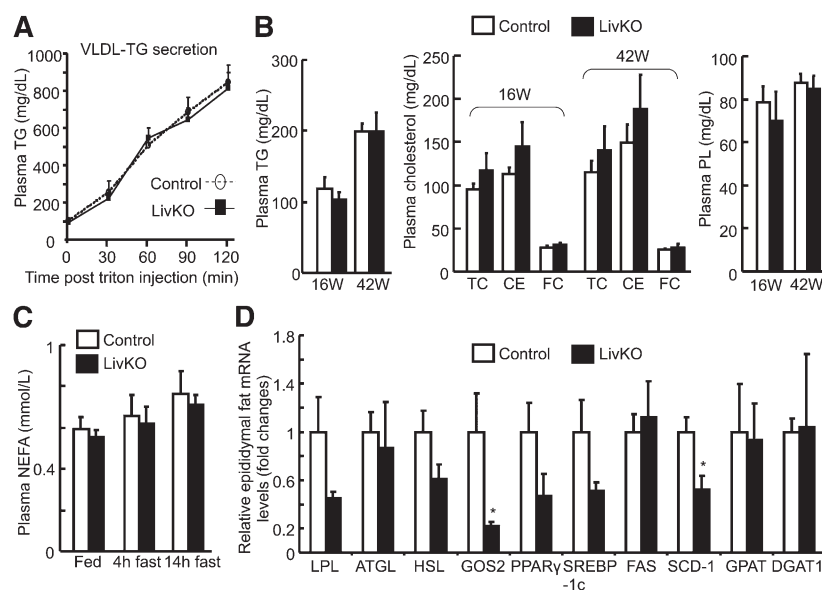

Fig. 3. Normal hepatic VLDL-TG production and unaltered plasma lipid concentrations in LivKO mice. A: Hepatic VLDL-TG secretion calculated as plasma accumulation of TG in chow-fed 8–10 week old males (n = 5) after tail vein injection of Triton WR1339. B: Plasma lipid concentrations in LivKO and control male mice at necropsy (n = 4–5). The plasma concentration of CE was calculated by multiplying the mass difference between TC and FC by 1.67. 16W, 16 weeks; 42W, 42 weeks. C: Plasma concentrations of NEFAs in LivKO and control mice at 38–42 weeks during fed state or after a 4 or 14 h fast (n = 4–5). D: Relative epididymal fat mRNA levels of genes related to lipolysis and lipogenesis in 42-week-old LivKO and control mice determined by qPCR (n = 4). GAPDH was used as an internal invariant control. *$P < 0.05$.
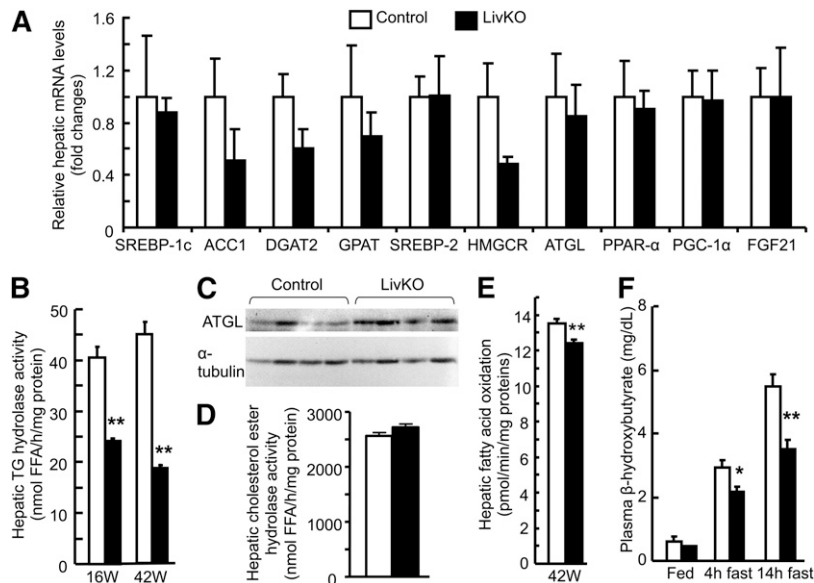
Fig. 4. LivKO mice show reduced hepatic TG hydrolase activity and FA oxidation. A: Relative hepatic mRNA levels of genes involved in lipid synthesis, hydrolysis, and regulation of FA oxidation. B: Hepatic TG hydrolase activity in 16 week (16W) and 42 week (42W) old LivKO and control mice (n = 4–5). C: Western blots of hepatic ATGL protein and a loading control α-tubulin. D: Hepatic CE hydrolase activity in 42-week-old LivKO and control mice (n = 4–5). E: FA oxidation in liver homogenates in 42-week-old mice (n = 4). F: Plasma concentrations of a ketone body β-hydroxybutyrate in LivKO and control mice at 38–42 weeks during fed state or after a 4 or 14 h fast (n = 4–5). ACC1, acetyl-CoA carboxylase 1; HMGCR, 3-hydroxy-3-methylglutaryl reductase; PGC-1α, PPAR-γ coactivator 1α; FGF21, fibroblast growth factor 21. *$P < 0.05$; **$P < 0.01$.

FFA/h/mg protein in LivKO vs. 44.9 ± 1.98 nmol FFA/h/mg protein in control). The reduction of hepatic TG hydrolase activity was not associated with a decrease in hepatic ATGL mRNA (Fig. 4A) or protein (Fig. 4C). Additionally, the cholesterol esterase activity remained unaltered in the LivKO liver homogenates (Fig. 4D). These findings suggest a critical role of CGI-58 in liver TG, but not CE hydrolysis.

TG hydrolysis-derived FFAs or their metabolites may serve as endogenous ligands for PPAR-α (55), a master regulator of FA oxidation. We found that hepatic inactivation of CGI-58 reduced hepatic FA oxidation activity by ∼9% (Fig. 4E). This reduction, though modest, was statistically significant. Consistently, the plasma concentration of β-hydroxybutyrate, an indicator of hepatic FA oxidation, fell significantly in LivKO mice that had been fasted for 4 or 14 h (Fig. 4F). There were no differences in plasma β-hydroxybutyrate concentrations between LivKO and control mice in the fed state. The mean plasma values of β-hydroxybutyrate were 0.44 ± 0.03 mg/dl, 2.18 ± 0.15 mg/dl, and 3.52 ± 0.28 mg/dl in fed, 4 h-fasted, and 14 h-fasted LivKO mice, respectively, whereas these values were 0.62 ± 0.12 mg/dl, 2.92 ± 0.26 mg/dl, and 5.48 ± 0.55 mg/dl in the respective control mice.

LivKO mice are not insulin resistant despite severe steatosis

Hepatic steatosis is often associated with insulin resistance (56). To examine whether hepatic steatosis induced by CGI-58 deficiency in the liver influences systemic insulin sensitivity, plasma glucose and insulin levels were analyzed, and glucose and insulin tolerance tests were performed.

The glucose and insulin concentrations were indistinguishable between LivKO and control mice at 38 weeks of age, regardless of fed or fasted state (**Fig. 5A**). LivKO relative to control mice at 39 weeks were not insulin resistant, and they appeared to tolerate glucose better within 30 min post glucose injection (Fig. 5B). When 8–12-week-old LivKO and control littermates on chow diet were used for acute insulin signaling assessment, the insulin-stimulated phosphorylation of Akt at threonine 308 was similar between the two groups (Fig. 5C), despite a 4-fold increase in hepatic TG content (873 ± 192 μg/mg protein in LivKO mice vs. 223 ± 30 μg/mg protein in control mice, n = 6, $P = 0.007$).

LivKO mice develop progressive steatohepatitis and hepatic fibrosis

Hepatic steatosis does not always progress to steatohepatitis and fibrosis (9, 10). To examine if hepatic steatosis induced by CGI-58 inactivation progresses to advanced stages of NAFLD over time, liver specimens from 16 and 42-week-old mice were stained by H and E and trichrome, and the histopathological alterations such as steatosis, lobular inflammation, and hepatocellular ballooning were scaled as described by Kleiner et al. (57). Liver CGI-58 inactivation induced modest steatosis at 16 weeks and significant steatosis at 42 weeks (Fig. 2A). Hepatocyte swelling (Fig. 2A), Mallory hyalin (not shown), lobular inflammation (Fig. 2A and **Fig. 6A**), and pericellular fibrosis (Fig. 6B) were also noted at 42 weeks.

In line with progressive development of steatohepatitis and liver fibrosis, the hepatic mRNA levels of two proinflammatory genes, tumor necrosis factor α and interleukin-1β,
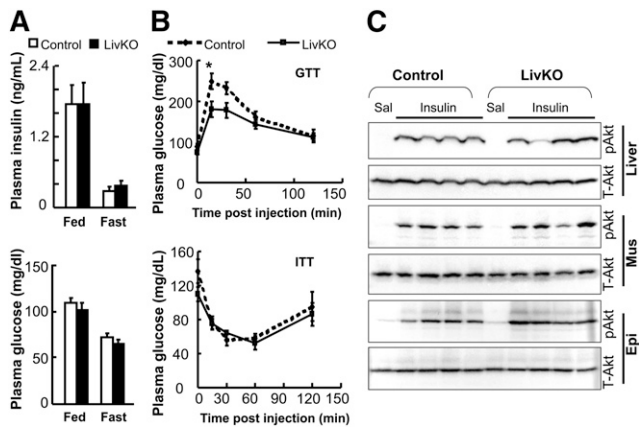
Fig. 5. LivKO mice are not insulin resistant. A: The 38 week old LivKO mice versus control male mice showed no changes in plasma concentrations of insulin and glucose in the fed or 14 h fast state (n = 4–5). B: Blood glucose levels in male mice subjected to GTT (at 39 weeks) and ITT (at 40 weeks) (n = 4–5). It appears that LivKO relative control mice tolerated glucose challenge better. C: Acute insulin signaling. The 8–12-week-old LivKO mice and control male littermates were anesthetized and injected with saline (Sal) or human insulin at 0.5 U/kg body weight via the portal vein. Liver, epididymal fat pad (Epi), and quadriceps muscle (Mus) were sequentially collected 5 min after insulin injection and snap-frozen in liquid nitrogen. The insulin-stimulated phosphorylation of Akt threonine 308 (pAkt) and total Akt (T-Akt) in these tissues were detected by immunoblotting using antibodies from Cell Signaling. *$P < 0.05$.

were similar between the two genotypes at 16 weeks, but dramatically elevated by about 18-fold and 3-fold, respectively, in LivKO mice at 42 weeks (Fig. 6C). Similarly, hepatic mRNA levels of fibrosis markers α-smooth muscle actin and collagen type 1 α1 remained unaltered at 16 weeks, but increased about 4-fold and 24-fold, respectively, in 42-week-old LivKO mice (Fig. 6C).

In addition, the liver damage was severe in 42-week-old LivKO mice, as evidenced by a significant elevation in the plasma enzymatic activities of both ALT and AST (Fig. 6D).

To determine if CGI-58 deficiency-induced fat deposition in the liver is associated with the existence of some factors known to trigger the progression of simple steatosis to steatohepatitis and liver fibrosis in LivKO mice, such as oxidative stress and ER stress, we measured hepatic superoxide production, redox state, and ER stress markers. It has been shown that DHE is converted to the red fluorescence product after specific reactions with intracellular superoxide, which is then irreversibly bound to double-strand DNA and shown as punctuate nuclear staining (58). DHE staining showed a dramatic increase in DHE fluorescence on liver cryosections from 42-week-old LivKO mice (Fig. 6E), indicating increased superoxide production. Consistently, the GSH/GSSG ratio, an indicator of cell's redox state, markedly decreased in the livers of these animals (Fig. 6F). Furthermore, the hepatic content of MDA, a product of lipid peroxidation, as TBARS, dramatically increased in the 42-week-old LivKO mice (Fig. 6F). No changes in hepatic GSH/GSSG ratio and TBARS content were observed in 16-week-old LivKO mice (data not shown).

CGI-58-induced hepatic steatosis did not cause ER stress because we observed no changes in hepatic levels of ER stress

protein markers such as two ER chaperones binding immunoglobulin protein (BiP) (also known as 78 kDa glucose-regulated protein GRP78) and protein disulfide isomerase, the serine/threonine kinase IRE1α, phosphorylated-IRE1α, endoplasmic oxidoreductin-1-like α, CHOP (a C/EBP-homologous protein), and protein kinase-like ER kinase in the 42-week-old LivKO mice (**Fig. 7A**). Additionally, ER stress-associated XBP-1 splicing did not occur (Fig. 7B), and mRNA levels for activating transcription factor 6, CHOP, and BiP did not increase (Fig. 7C) in the livers of these animals.

Recently, cholesterol accumulation in liver mitochondria was shown to play a crucial role in the progression of steatosis to steatohepatitis and fibrosis (59). Considering increased cholesterol in the LivKO mouse liver, we isolated hepatic mitochondria as our colleague Dr. M. Colombini has described (60), and measured mitochondrial TC by gas chromatography. We found no significant increases in hepatic mitochondrial cholesterol content between LivKO and control mice (data not shown).

DISCUSSION

The present study demonstrates that liver-specific inactivation of CGI-58 in mice directly causes advanced stages of NAFLD over time, indicating a local and key role of liver CGI-58 on NAFLD development and progression. Deficiency of liver CGI-58 substantially reduces hepatic TG hydrolase activity without altering hepatic VLDL-TG secretion and hepatic expression levels of genes related to de novo lipid synthesis, and suggests an important role of CGI-58-dependent intracellular TG hydrolysis in the pathogenesis of NAFLD.

The CGI-58 LivKO mouse line appears to be a useful animal model for exploring molecular insights into NAFLD progression. CGI-58 LivKO mice showed hepatic steatosis at 3 weeks of age. The hepatic steatosis worsened at 16 weeks, but hepatic inflammation and fibrosis were minimal at this stage. At 42 weeks, LivKO mice displayed obvious steatohepatitis and hepatic fibrosis. The plasma levels of ALT and AST, two markers of liver damage, increased significantly at this time. These observations demonstrate that steatohepatitis and fibrosis are natural histopathological consequences of CGI-58 deficiency-induced hepatic steatosis. Some human subjects with hepatic steatosis never developed advanced NAFLD over time (9, 10). Perhaps, the etiology of hepatic steatosis in these individuals is not related to deficiency of CGI-58-mediated cellular TG hydrolysis.

Our data support a role of increased oxidative stress (Fig. 6E, F), but not ER stress, in the age-related development of steatohepatitis and liver fibrosis in LivKO mice. Certainly, other mechanisms may exist. Early studies using fibroblasts from a CDS patient identified a defect of these fibroblasts in TG recycling to PLs (61). This in vitro study suggests a potential role of CGI-58 in regulating cellular PL homeostasis in vivo. We found that hepatic total PLs were significantly reduced in 42-week-old LivKO mice
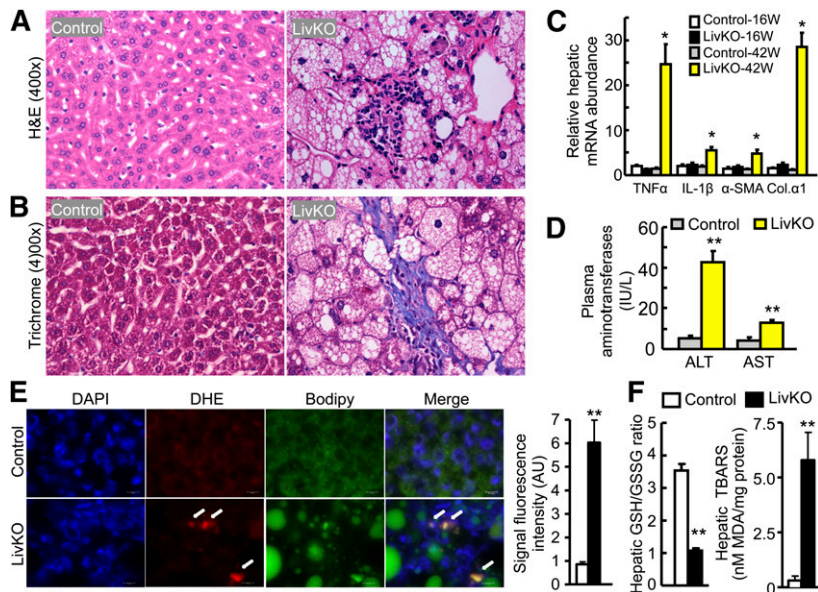
Fig. 6. LivKO mice at 42 weeks display steatohepatitis, hepatic fibrosis, and increased hepatic oxidative stress. A: H and E staining of liver sections from LivKO and control male mice. Inflammatory infiltration in the steatotic region of the knockout liver is shown. B: Trichrome staining of liver sections from LivKO and control males, showing centrilobular and pericellular fibrosis. C: Hepatic mRNAs for genes related to inflammation and fibrosis in 16 and 42 week-old LivKO and control male mice (n = 4). Cyclophilin was used as an internal invariant control. TNFα, tumor necrosis factor α; IL-1β, interleukin-1β; α-SMA, α-smooth muscle actin; Col.α1, collagen type 1 α1. D: Liver damage in 42-week-old LivKO mice (n = 4–5) as evidenced by increased plasma concentrations of AST and ALT. E: Hepatic superoxide production. Unfixed liver cryosections (10 μm thick) were stained DHE (5 μM, 30 min) for superoxide (red). Nuclei were stained with DAPI (blue). LDs were stained with Bodipy (green). White arrows indicate superoxide accumulation in liver tissue. Scale bars: 10 μm. Signal fluorescence intensity of ten randomly selected 63× microscopic fields from each group was quantified using Image J software (National Institutes of Health). F: Increased oxidative stress. Hepatic GSH/GSSG ratio and TBARS were determined as described in Materials and Methods (n = 4). *$P < 0.05$ and **$P < 0.01$ (vs. control mice of the same age).

(Fig. 2B). Although PL reduction might be a consequence of steatohepatitis and hepatic fibrogenesis in CGI-58 LivKO mice, this reduction has the potential to directly facilitate the progression of NAFLD. For instance, several recent studies have demonstrated a critical role of PL homeostasis in the development of NASH and in the control of LD sizes (62, 63). In the absence of CGI-58, the uncontrolled expansion of LD size may mechanically and/or biochemically cause damage to hepatocytes, thereby generating some of the second hit factors (10) to promote the transition of simple steatosis to NASH.

Hepatic TG hydrolase activity decreased 40–58% in CGI-58 LivKO mice compared with controls (Fig. 4B). In liver-specific ATGL knockout mice, this activity decreases ∼65% (18), which is comparable to that seen in CGI-58 LivKO mice, suggesting that ATGL may account for the decreased TG hydrolase activity in the CGI-58-deficient liver. The preservation of ∼50% TG hydrolase activity in both CGI-58-null and ATGL-null livers indicates that other TG hydrolases exist in the liver, such as TG Hydrolase (TGH) (64), but they may not be the targets of CGI-58. Consistent with this, addition of recombinant GST-CGI-58 to ATGL-deficient liver lysates only leads to a marginal increase (1.2-fold) in hepatic TG hydrolase activity (42). Nonetheless, data from CGI-58 and ATGL knockout livers indicate that an ∼50% reduction in hepatic TG hydrolysis

is sufficient to cause progressive hepatic steatosis. Other lipases are seemingly not able to compensate for TG hydrolysis inhibition induced by the loss of ATGL or CGI-58.
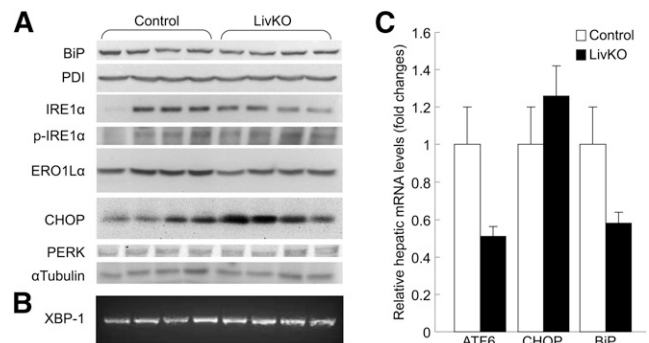

Fig. 7. LivKO mice at 42 weeks exhibit no hepatic ER stress. A: Western blots of liver proteins related to ER stress. α-Tubulin was used as a loading control. B: XBP-1 splicing assay by reverse transcriptase PCR using total hepatic RNAs. C: Hepatic mRNA levels of ER stress-responsive genes activating transcription factor 6 (ATF6), CHOP, and BiP measured by qPCR. Cyclophilin was used as an internal invariant control. PDI, protein disulfide isomerase; PERK, protein kinase-like endoplasmic reticulum kinase; p-IRE1α, phosphorylated-IRE1α; ERO1Lα, endoplasmic oxidoreductin-1-like α.
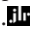
Although CGI-58 may function through ATGL in the liver to promote cellular TG hydrolysis (25, 42), mice with liver-specific inactivation of ATGL showed no signs of steatohepatitis and hepatic fibrosis, even at 12 months of age, despite progressive hepatic steatosis (18). Additionally, the hepatic TG content elevated only ~3-fold in the 4–12 month old liver ATGL knockout mice relative to control mice of the same age on a chow diet (18). However, the hepatic TG content in the chow-fed CGI-58 LivKO mice increased 8-fold at 16 weeks and 52-fold at 42 weeks compared with the chow-fed control mice of the same age. These differences between the two models indicate that liver CGI-58 must have functions beyond activating ATGL. CGI-58-deficient liver accumulates both esterified and free cholesterol. Hepatic cholesterol was not reported in the ATGL-deficient liver (17, 18, 65). If we assume ATGL-deficient liver does not accumulate a significant amount of CE, or only accumulates FC in LDs, CE deposition in CGI-58 LivKO mice would suggest a stimulating role of CGI-58 in the hydrolysis of CEs. However, hepatic CE hydrolase activity was not altered in LivKO mice (Fig. 4D), suggesting that liver CGI-58 may not function as a coactivator of a cholesterol esterase, and that the hepatic accumulation of CE and FC may be a result of the sequestration of these hydrophobic molecules on the LDs in the liver of LivKO mice. Nevertheless, future studies are required to explore CGI-58's novel functions.

One metabolic fate of FFAs released from cytosolic TG hydrolysis is to enter the oxidative pathway. In line with this, hepatic FA oxidation rates and plasma concentrations of β-hydroxybutyrate (a marker of hepatic FA β-oxidation) fall significantly in CGI-58 LivKO mice. ASO-induced knockdown of CGI-58 in a few tissues of adult mice also reduces FA oxidation (43). A case study of a young female patient with CDS showed impaired long-chain FA oxidation and no detectable ketones in her blood or urine after a 24 h fast on three occasions (66). Another metabolic fate of FFAs released from cytosolic TG hydrolysis is to enter the reesterification pathway in the ER for the assembly of TG-rich VLDL particles. We have previously shown that ASO-induced simultaneous knockdown of CGI-58 in a few tissues (liver, fat, and macrophages) of adult mice causes hepatic steatosis and reduction in hepatic VLDL-TG secretion (43). However, this reduction in hepatic VLDL-TG secretion is not seen in LivKO mice, suggesting that knockdown of CGI-58 in other tissues may have indirect effects on hepatic VLDL production.

Numerous animal and human studies have shown a strong association of hepatic steatosis with insulin resistance (56, 67). However, liver CGI-58 deficiency-induced NAFLD does not appear to alter systemic insulin sensitivity and tissue insulin signaling transduction. Dissociation of hepatic steatosis and insulin resistance was reported in other animal models and human subjects (2). For example, mice overexpressing DGAT2 in liver accumulate TG in liver, but show no signs of insulin resistance (68). Deficiency of liver ATGL does not induce insulin resistance, despite causing progressive hepatic steatosis (18). The whole-body ATGL knockout mice exhibit fat accumulation in most tissues, yet are more insulin sensitive (17). Two previous studies including ours showed that CGI-58 knockdown induced by ASO increases systemic insulin sensitivity in adult mice, though causing fatty liver and accumulation of DAGs (43, 69), known insulin signaling-suppressing lipids (56). Perhaps how and where fat is accumulated is more important than how much fat is accumulated in altering cell's insulin sensitivity. Accumulated TG-rich LDs in cytosol or altered subcellular compartments in CGI-58-deficient hepatocytes may directly sequester insulin signaling-suppressing lipids and prevent them from gaining access to the insulin signaling pathway (43, 69). Alternatively, the expanded cellular TG pool may sequester excess FFAs away from metabolic pathways responsible for generation of insulin signaling-suppressing or lipotoxicity-inducing metabolites, which would be consistent with a study showing that cellular TG accumulation protects cultured cells against FA-induced lipotoxicity (70).

Interestingly, although DAGs were accumulated in the liver of CGI-58 antisense olionucleotide-treated mice in which CGI-58 was simultaneously knocked down in a few tissues (43, 69), liver-specific deletion of CGI-58 in mice caused no deposition of DAGs in the liver (Table 2). This finding suggests that increased hepatic DAGs in CGI-58 ASO-treated mice may result from metabolic reprogramming of liver in response to CGI-58 inhibition in other tissues. Alternatively, the time point difference in inhibiting CGI-58 expression between the present study (genetic deletion early in life) and the two previous studies (knockdown in adult mice) may have contributed to the distinct hepatic DAG content.

In conclusion, liver CGI-58 protects against hepatic steatosis, NASH, and hepatic fibrosis in mice. The liver-specific CGI-58 knockout mouse line may be a good model for probing molecular mechanisms underlying NAFLD progression. This model may be useful in exploring preventive and therapeutic approaches for NAFLD.⬛

REFERENCES

1. Unger, R. H. 2002. Lipotoxic diseases. *Annu. Rev. Med.* **53:** 319–336.
2. Cohen, J. C., J. D. Horton, and H. H. Hobbs. 2011. Human fatty liver disease: old questions and new insights. *Science.* **332:** 1519–1523.
3. Schaffner, F., and H. Thaler. 1986. Nonalcoholic fatty liver disease. *Prog. Liver Dis.* **8:** 283–298.
4. Angulo, P. 2002. Nonalcoholic fatty liver disease. *N. Engl. J. Med.* **346:** 1221–1231.
5. Browning, J. D., L. S. Szczepaniak, R. Dobbins, P. Nuremberg, J. D. Horton, J. C. Cohen, S. M. Grundy, and H. H. Hobbs. 2004. Prevalence of hepatic steatosis in an urban population in the United States: impact of ethnicity. *Hepatology.* **40:** 1387–1395.
6. Clark, J. M. 2006. The epidemiology of nonalcoholic fatty liver disease in adults. *J. Clin. Gastroenterol.* **40(Suppl 1):** S5–S10.
7. Browning, J. D., and J. D. Horton. 2004. Molecular mediators of hepatic steatosis and liver injury. *J. Clin. Invest.* **114:** 147–152.
8. Brunt, E. M., D. E. Kleiner, L. A. Wilson, P. Belt, and B. A. Neuschwander-Tetri. 2011. Nonalcoholic fatty liver disease (NAFLD) activity score and the histopathologic diagnosis in NAFLD: distinct clinicopathologic meanings. *Hepatology.* **53:** 810–820.

9. Teli, M. R., O. F. James, A. D. Burt, M. K. Bennett, and C. P. Day. 1995. The natural history of nonalcoholic fatty liver: a follow-up study. *Hepatology.* **22:** 1714–1719.

10. Day, C. P., and O. F. James. 1998. Steatohepatitis: a tale of two "hits"? *Gastroenterology.* **114:** 842–845.

11. Koteish, A., and A. M. Diehl. 2001. Animal models of steatosis. *Semin. Liver Dis.* **21:** 89–104.

12. Tiniakos, D. G., M. B. Vos, and E. M. Brunt. 2010. Nonalcoholic fatty liver disease: pathology and pathogenesis. *Annu. Rev. Pathol.* **5:** 145–171.

13. Hebbard, L., and J. George. 2011. Animal models of nonalcoholic fatty liver disease. *Nat. Rev. Gastroenterol. Hepatol.* **8:** 35–44.

14. Zimmermann, R., J. G. Strauss, G. Haemmerle, G. Schoiswohl, R. Birner-Gruenberger, M. Riederer, A. Lass, G. Neuberger, F. Eisenhaber, A. Hermetter, et al. 2004. Fat mobilization in adipose tissue is promoted by adipose triglyceride lipase. *Science.* **306:** 1383–1386.

15. Villena, J. A., S. Roy, E. Sarkadi-Nagy, K. H. Kim, and H. S. Sul. 2004. Desnutrin, an adipocyte gene encoding a novel patatin domain-containing protein, is induced by fasting and glucocorticoids: ectopic expression of desnutrin increases triglyceride hydrolysis. *J. Biol. Chem.* **279:** 47066–47075.

16. Jenkins, C. M., D. J. Mancuso, W. Yan, H. F. Sims, B. Gibson, and R. W. Gross. 2004. Identification, cloning, expression, and purification of three novel human calcium-independent phospholipase A2 family members possessing triacylglycerol lipase and acylglycerol transacylase activities. *J. Biol. Chem.* **279:** 48968–48975.

17. Haemmerle, G., A. Lass, R. Zimmermann, G. Gorkiewicz, C. Meyer, J. Rozman, G. Heldmaier, R. Maier, C. Theussl, S. Eder, et al. 2006. Defective lipolysis and altered energy metabolism in mice lacking adipose triglyceride lipase. *Science.* **312:** 734–737.

18. Wu, J. W., S. P. Wang, F. Alvarez, S. Casavant, N. Gauthier, L. Abed, K. G. Soni, G. Yang, and G. A. Mitchell. 2011. Deficiency of liver adipose triglyceride lipase in mice causes progressive hepatic steatosis. *Hepatology.* **54:** 122–132.

19. Reid, B. N., G. P. Ables, O. A. Otlivanchik, G. Schoiswohl, R. Zechner, W. S. Blaner, I. J. Goldberg, R. F. Schwabe, S. C. Chua, Jr., and L. S. Huang. 2008. Hepatic overexpression of hormone-sensitive lipase and adipose triglyceride lipase promotes fatty acid oxidation, stimulates direct release of free fatty acids, and ameliorates steatosis. *J. Biol. Chem.* **283:** 13087–13099.

20. Turpin, S. M., A. J. Hoy, R. D. Brown, C. G. Rudaz, J. Honeyman, M. Matzaris, and M. J. Watt. 2011. Adipose triacylglycerol lipase is a major regulator of hepatic lipid metabolism but not insulin sensitivity in mice. *Diabetologia.* **54:** 146–156.

21. Lai, C. H., C. Y. Chou, L. Y. Ch'ang, C. S. Liu, and W. Lin. 2000. Identification of novel human genes evolutionarily conserved in Caenorhabditis elegans by comparative proteomics. *Genome Res.* **10:** 703–713.

22. Schrag, J. D., and M. Cygler. 1997. Lipases and alpha/beta hydrolase fold. *Methods Enzymol.* **284:** 85–107.

23. Simon, G. M., and B. F. Cravatt. 2006. Endocannabinoid biosynthesis proceeding through glycerophospho-N-acyl ethanolamine and a role for alpha/beta-hydrolase 4 in this pathway. *J. Biol. Chem.* **281:** 26465–26472.

24. Subramanian, V., A. Rothenberg, C. Gomez, A. W. Cohen, A. Garcia, S. Bhattacharyya, L. Shapiro, G. Dolios, R. Wang, M. P. Lisanti, et al. 2004. Perilipin A mediates the reversible binding of CGI-58 to lipid droplets in 3T3-L1 adipocytes. *J. Biol. Chem.* **279:** 42062–42071.

25. Lass, A., R. Zimmermann, G. Haemmerle, M. Riederer, G. Schoiswohl, M. Schweiger, P. Kienesberger, J. G. Strauss, G. Gorkiewicz, and R. Zechner. 2006. Adipose triglyceride lipase-mediated lipolysis of cellular fat stores is activated by CGI-58 and defective in Chanarin-Dorfman syndrome. *Cell Metab.* **3:** 309–319.

26. Brown, J. M., S. Chung, A. Das, G. Shelness, L. L. Rudel, and L. Yu. 2007. CGI-58 facilitates mobilization of cytoplasmic triglyceride for lipoprotein secretion in hepatoma cells. *J. Lipid Res.* **48:** 2295–2305.

27. Lefèvre, C., F. Jobard, F. Caux, B. Bouadjar, A. Karaduman, R. Heilig, H. Lakhdar, A. Wollenberg, J. L. Verret, J. Weissenbach, et al. 2001. Mutations in CGI-58, the gene encoding a new protein of the esterase/lipase/thioesterase subfamily, in Chanarin-Dorfman syndrome. *Am. J. Hum. Genet.* **69:** 1002–1012.

28. Yamaguchi, T., N. Omatsu, E. Morimoto, H. Nakashima, K. Ueno, T. Tanaka, K. Satouchi, F. Hirose, and T. Osumi. 2007. CGI-58 facilitates lipolysis on lipid droplets but is not involved in the vesiculation of lipid droplets caused by hormonal stimulation. *J. Lipid Res.* **48:** 1078–1089.

29. Chanarin, I., A. Patel, G. Slavin, E. J. Wills, T. M. Andrews, and G. Stewart. 1975. Neutral-lipid storage disease: a new disorder of lipid metabolism. *BMJ.* **1:** 553–555.

30. Dorfman, M. L., C. Hershko, S. Eisenberg, and F. Sagher. 1974. Ichthyosiform dermatosis with systemic lipidosis. *Arch. Dermatol.* **110:** 261–266.

31. Jordans, G. H. 1953. The familial occurrence of fat containing vacuoles in the leukocytes diagnosed in two brothers suffering from dystrophia musculorum progressiva (ERB.). *Acta Med. Scand.* **145:** 419–423.

32. Rozenszajn, L., A. Klajman, D. Yaffe, and P. Efrati. 1966. Jordans' anomaly in white blood cells. Report of case. *Blood.* **28:** 258–265.

33. Slavin, G., E. J. Wills, J. E. Richmond, I. Chanarin, T. Andrews, and G. Stewart. 1975. Morphological features in a neutral lipid storage disease. *J. Clin. Pathol.* **28:** 701–710.

34. Igal, R. A., J. M. Rhoads, and R. A. Coleman. 1997. Neutral lipid storage disease with fatty liver and cholestasis. *J. Pediatr. Gastroenterol. Nutr.* **25:** 541–547.

35. Gürakan, F., F. Kaymaz, N. Kocak, U. Ors, A. Yüce, and N. Atakan. 1999. A cause of fatty liver: neutral lipid storage disease with ichthyosis–electron microscopic findings. *Dig. Dis. Sci.* **44:** 2214–2217.

36. Srinivasan, R., N. Hadzic, J. Fischer, and A. S. Knisely. 2004. Steatohepatitis and unsuspected micronodular cirrhosis in Dorfman-Chanarin syndrome with documented ABHD5 mutation. *J. Pediatr.* **144:** 662–665.

37. Bruno, C., E. Bertini, M. Di Rocco, D. Cassandrini, G. Ruffa, T. De Toni, M. Seri, M. Spada, G. Li Volti, A. D'Amico, et al. 2008. Clinical and genetic characterization of Chanarin-Dorfman syndrome. *Biochem. Biophys. Res. Commun.* **369:** 1125–1128.

38. Miranda, A., S. DiMauro, A. Eastwood, A. Hays, W. G. Johnson, M. Olarte, R. Whitlock, R. Mayeux, and L. P. Rowland. 1979. Lipid storage myopathy, ichthyosis, and steatorrhea. *Muscle Nerve.* **2:** 1–13.

39. Ciesek, S., J. Hadem, J. Fischer, M. P. Manns, and C. P. Strassburg. 2006. A rare cause of nonalcoholic fatty liver disease. *Ann. Intern. Med.* **145:** 154–155.

40. Ronchetti, A., D. Prati, M. G. Pezzotta, D. Tavian, R. Colombo, F. Callea, and A. Colli. 2008. Severe steatohepatitis in a patient with a rare neutral lipid storage disorder due to ABHD5 mutation. *J. Hepatol.* **49:** 474–477.

41. Fischer, J., C. Lefevre, E. Morava, J. M. Mussini, P. Laforet, A. Negre-Salvayre, M. Lathrop, and R. Salvayre. 2007. The gene encoding adipose triglyceride lipase (PNPLA2) is mutated in neutral lipid storage disease with myopathy. *Nat. Genet.* **39:** 28–30.

42. Radner, F. P., I. E. Streith, G. Schoiswohl, M. Schweiger, M. Kumari, T. O. Eichmann, G. Rechberger, H. C. Koefeler, S. Eder, S. Schauer, et al. 2010. Growth retardation, impaired triacylglycerol catabolism, hepatic steatosis, and lethal skin barrier defect in mice lacking comparative gene identification-58 (CGI-58). *J. Biol. Chem.* **285:** 7300–7311.

43. Brown, J. M., J. L. Betters, C. Lord, Y. Ma, X. Han, K. Yang, H. M. Alger, J. Melchior, J. Sawyer, R. Shah, et al. 2010. CGI-58 knockdown in mice causes hepatic steatosis but prevents diet-induced obesity and glucose intolerance. *J. Lipid Res.* **51:** 3306–3315.

44. Nagy, A., J. Rossant, R. Nagy, W. Abramow-Newerly, and J. C. Roder. 1993. Derivation of completely cell culture-derived mice from early-passage embryonic stem cells. *Proc. Natl. Acad. Sci. USA.* **90:** 8424–8428.

45. Yu, L., R. E. Hammer, J. Li-Hawkins, K. Von Bergmann, D. Lutjohann, J. C. Cohen, and H. H. Hobbs. 2002. Disruption of Abcg5 and Abcg8 in mice reveals their crucial role in biliary cholesterol secretion. *Proc. Natl. Acad. Sci. USA.* **99:** 16237–16242.

46. Yang, J., J. L. Goldstein, R. E. Hammer, Y. A. Moon, M. S. Brown, and J. D. Horton. 2001. Decreased lipid synthesis in livers of mice with disrupted site-1 protease gene. *Proc. Natl. Acad. Sci. USA.* **98:** 13607–13612.

47. Temel, R. E., W. Tang, Y. Ma, L. L. Rudel, M. C. Willingham, Y. A. Ioannou, J. P. Davies, L. M. Nilsson, and L. Yu. 2007. Hepatic Niemann-Pick C1-like 1 regulates biliary cholesterol concentration and is a target of ezetimibe. *J. Clin. Invest.* **117:** 1968–1978.

48. Zhou, D., D. Samovski, A. L. Okunade, P. D. Stahl, N. A. Abumrad, and X. Su. 2012. CD36 level and trafficking are determinants of lipolysis in adipocytes. *FASEB J.* **26:** 4733–4742.

49. Jia, L., Y. Ma, S. Rong, J. L. Betters, P. Xie, S. Chung, N. Wang, W. Tang, and L. Yu. 2010. Niemann-Pick C1-like 1 deletion in mice prevents high-fat diet-induced fatty liver by reducing lipogenesis. *J. Lipid Res.* **51:** 3135–3144.

50. Holm, C., and T. Osterlund. 1999. Hormone-sensitive lipase and neutral cholesteryl ester lipase. *Methods Mol. Biol.* **109:** 109–121.

51. Deng, Y., Z. V. Wang, C. Tao, N. Gao, W. L. Holland, A. Ferdous, J. J. Repa, G. Liang, J. Ye, M. A. Lehrman, et al. 2013. The Xbp1s/GalE axis links ER stress to postprandial hepatic metabolism. *J. Clin. Invest.* **123:** 455–468.

52. Postic, C., M. Shiota, K. D. Niswender, T. L. Jetton, Y. Chen, J. M. Moates, K. D. Shelton, J. Lindner, A. D. Cherrington, and M. A. Magnuson. 1999. Dual roles for glucokinase in glucose homeostasis as determined by liver and pancreatic beta cell-specific gene knock-outs using Cre recombinase. *J. Biol. Chem.* **274:** 305–315.

53. Brown, J. M., S. Chung, A. Das, G. S. Shelness, L. L. Rudel, and L. Yu. 2007. CGI-58 facilitates the mobilization of cytoplasmic triglyceride for lipoprotein secretion in hepatoma cells. *J. Lipid Res.* **48:** 2295–2305.

54. Yang, X., X. Lu, M. Lombes, G. B. Rha, Y. I. Chi, T. M. Guerin, E. J. Smart, and J. Liu. 2010. The G(0)/G(1) switch gene 2 regulates adipose lipolysis through association with adipose triglyceride lipase. *Cell Metab.* **11:** 194–205.

55. Haemmerle, G., T. Moustafa, G. Woelkart, S. Buttner, A. Schmidt, T. van de Weijer, M. Hesselink, D. Jaeger, P. C. Kienesberger, K. Zierler, et al. 2011. ATGL-mediated fat catabolism regulates cardiac mitochondrial function via PPAR-alpha and PGC-1. *Nat. Med.* **17:** 1076–1085.

56. Samuel, V. T., and G. I. Shulman. 2012. Mechanisms for insulin resistance: common threads and missing links. *Cell.* **148:** 852–871.

57. Kleiner, D. E., E. M. Brunt, M. Van Natta, C. Behling, M. J. Contos, O. W. Cummings, L. D. Ferrell, Y. C. Liu, M. S. Torbenson, A. Unalp-Arida, et al. 2005. Design and validation of a histological scoring system for nonalcoholic fatty liver disease. *Hepatology.* **41:** 1313–1321.

58. Zhao, H., S. Kalivendi, H. Zhang, J. Joseph, K. Nithipatikom, J. Vasquez-Vivar, and B. Kalyanaraman. 2003. Superoxide reacts with hydroethidine but forms a fluorescent product that is distinctly different from ethidium: potential implications in intracellular fluorescence detection of superoxide. *Free Radic. Biol. Med.* **34:** 1359–1368.

59. Marí, M., F. Caballero, A. Colell, A. Morales, J. Caballeria, A. Fernandez, C. Enrich, J. C. Fernandez-Checa, and C. Garcia-Ruiz. 2006. Mitochondrial free cholesterol loading sensitizes to TNF- and Fas-mediated steatohepatitis. *Cell Metab.* **4:** 185–198.

60. Stiban, J., D. Fistere, and M. Colombini. 2006. Dihydroceramide hinders ceramide channel formation: Implications on apoptosis. *Apoptosis.* **11:** 773–780.

61. Igal, R. A., and R. A. Coleman. 1996. Acylglycerol recycling from triacylglycerol to phospholipid, not lipase activity, is defective in neutral lipid storage disease fibroblasts. *J. Biol. Chem.* **271:** 16644–16651.

62. Li, Z., L. B. Agellon, T. M. Allen, L. Umeda, L. Jewell, A. Mason, and D. E. Vance. 2006. The ratio of phosphatidylcholine to phosphatidylethanolamine influences membrane integrity and steatohepatitis. *Cell Metab.* **3:** 321–331.

63. Krahmer, N., Y. Guo, F. Wilfling, M. Hilger, S. Lingrell, K. Heger, H. W. Newman, M. Schmidt-Supprian, D. E. Vance, M. Mann, et al. 2011. Phosphatidylcholine synthesis for lipid droplet expansion is mediated by localized activation of CTP:phosphocholine cytidylyltransferase. *Cell Metab.* **14:** 504–515.

64. Lehner, R., Z. Cui, and D. E. Vance. 1999. Subcellullar localization, developmental expression and characterization of a liver triacylglycerol hydrolase. *Biochem. J.* **338:** 761–768.

65. Fuchs, C. D., T. Claudel, P. Kumari, G. Haemmerle, M. J. Pollheimer, T. Stojakovic, H. Scharnagl, E. Halilbasic, J. Gumhold, D. Silbert, et al. 2012. Absence of adipose triglyceride lipase protects from hepatic endoplasmic reticulum stress in mice. *Hepatology.* **56:** 270–280.

66. Angelini, C., M. Philippart, C. Borrone, N. Bresolin, M. Cantini, and S. Lucke. 1980. Multisystem triglyceride storage disorder with impaired long-chain fatty acid oxidation. *Ann. Neurol.* **7:** 5–10.

67. Magkos, F., X. Su, D. Bradley, E. Fabbrini, C. Conte, J. C. Eagon, J. E. Varela, E. M. Brunt, B. W. Patterson, and S. Klein. 2012. Intrahepatic diacylglycerol content is associated with hepatic insulin resistance in obese subjects. *Gastroenterology.* **142:** 1444–1446.

68. Monetti, M., M. C. Levin, M. J. Watt, M. P. Sajan, S. Marmor, B. K. Hubbard, R. D. Stevens, J. R. Bain, C. B. Newgard, R. V. Farese, Sr., et al. 2007. Dissociation of hepatic steatosis and insulin resistance in mice overexpressing DGAT in the liver. *Cell Metab.* **6:** 69–78.

69. Cantley, J. L., T. Yoshimura, J. P. Camporez, D. Zhang, F. R. Jornayvaz, N. Kumashiro, F. Guebre-Egziabher, M. J. Jurczak, M. Kahn, B. A. Guigni, et al. 2013. CGI-58 knockdown sequesters diacylglycerols in lipid droplets/ER-preventing diacylglycerol-mediated hepatic insulin resistance. *Proc. Natl. Acad. Sci. USA.* **110:** 1869–1874.

70. Listenberger, L. L., X. Han, S. E. Lewis, S. Cases, R. V. Farese, Jr., D. S. Ory, and J. E. Schaffer. 2003. Triglyceride accumulation protects against fatty acid-induced lipotoxicity. *Proc. Natl. Acad. Sci. USA.* **100:** 3077–3082.